COMPARISON OF EXPERIMENTAL AND SIMULATION STUDIES IN THE STRENGTH ANALYSIS OF STRUCTURAL COMPONENTS: A CASE STUDY OF CHAMBERED TUBULAR STRUCTURES MANUFACTURED USING ADDITIVE TECHNOLOGY

Grzegorz SZALA[*], Karolina KAROLEWSKA[**], Maciej JANIEC[*]

[*]Faculty of Physics, Astronomy and Informatics, Nicolaus Copernicus University in Toruń, ul.Grudziądzka 5, 87-100 Toruń, Poland
[**]Faculty of Mechanical Engineering, PBS Bydgoszcz University of Science and Technology, al. Prof. S. Kaliskiego 7, 85-796 Bydgoszcz, Poland

szala@fizyka.umk.pl, karolina.karolewska@pbs.edu.pl, maciej.janiec@umk.pl

received 14 April 2026, revised 10 July 2026., accepted 10 July 2026

Abstract: This paper investigates the mechanical performance of thin-walled tubular structures with chambered (lattice) internal geometries manufactured from ABS using fused deposition modelling (FDM). The objective of the study was to evaluate the influence of infill geometry on load-bearing capacity and deformation behaviour under bending and compressive loading conditions and to compare lattice configurations with solid structures. Experimental investigations included three-point bending and axial compression tests performed using INSTRON testing machines. Four structural configurations were analysed: ladder-type, triangular, tubular, and solid. In addition, finite element method (FEM) simulations were conducted to investigate the displacement response of the structures under compressive loading. The experimental results showed that the solid structure achieved the highest load-bearing capacity but at the expense of increased mass. Among the lattice configurations, the ladder-type structure demonstrated the most favourable overall performance, reaching load levels close to those of the solid structure while reducing mass by more than 50%. The triangular structure provided intermediate performance, whereas the tubular configuration exhibited the lowest load-bearing capacity in both bending and compression tests. FEM simulations reproduced the displacement-response trends of the investigated geometries and provided qualitative insight into the influence of chamber geometry on structural behaviour. The results confirm that appropriately designed lattice structures can achieve a favourable load-bearing-capacity-to-weight ratio, making them attractive for lightweight engineering applications.

Key words: additive manufacturing, lattice structures, thin-walled pipes, mechanical properties, finite element method

1. INTRODUCTION

The structural resistance to external loads is one of the key issues in materials engineering and structural mechanics. It becomes particularly important in the case of components subjected to intensive service conditions, where they must withstand both static and dynamic loads [5, 9, 12]. Pipe conduits, widely used across various industrial sectors, are exposed to external forces such as bending and compression, as well as internal loads, including fluid and gas pressure [10, 16].

Traditionally used solid-walled pipes, although characterized by high strength, exhibit certain structural limitations, such as high mass and stiffness, which affect their resistance to variable loads and thermal stresses. For this reason, increasing attention is being given to chamber-structured conduits and lattice structures, which offer an optimal strength-to-weight ratio, as well as improved energy absorption capacity and resistance to material fatigue [1, 3, 6, 8].

Lattice structures are spatial systems composed of regularly arranged struts and nodes, forming an optimized material network. Their mechanical properties depend on geometry, load distribution, and the type of material used. Studies conducted by Zhang et al. demonstrated that lattice structures with octagonal and tetrahedral topologies exhibit higher compressive and bending strength compared to rectangular configurations. Experimental tests performed using the digital image correlation (DIC) method confirmed that the application of lattice structures enables a reduction in conduit weight by more than 40% while maintaining comparable mechanical properties to solid materials [17].

Yang et al. also conducted numerical and experimental studies on lattice pipes manufactured using selective laser melting (SLM), demonstrating that an appropriate configuration of the structure's geometry enhances resistance to impact and dynamic loads. Similar conclusions were reported by Li et al., who indicated that the application of topology optimization techniques enables the adaptation of lattice structures to specific application requirements, resulting in a significant improvement in mechanical properties while simultaneously reducing material consumption [7]. Topology optimization integrated with additive manufacturing enables the systematic design of lightweight structures with improved mechanical efficiency [33, 34].

Conventional manufacturing methods, such as CNC machining, casting, and forming, are limited in their ability to produce complex internal structures, including chambers and spatial lattices. Additive manufacturing technologies overcome these limitations by enabling the production of components with precisely controlled geometries that can be optimized for specific applications [2, 4, 8, 27, 30].

In the case of lattice and chambered structures, the application of 3D printing allows for a reduction in structural weight while maintaining adequate strength, tailoring of mechanical properties through modifications in lattice or chamber geometry, enhancement of cooling efficiency via optimized internal channels, and improved resistance to vibrations and dynamic loading [13, 18]. Recent advances in mechanical metamaterials demonstrate that architected lattice structures can achieve exceptional stiffness-to-weight ratios and tunable deformation mechanisms [31, 32].

The aerospace and space industries are among the primary sectors in which 3D printing of lattice and chambered structures plays a crucial role [15]. By reducing component weight, it is possible to decrease fuel consumption and improve flight efficiency [25,27]. Additive manufacturing technologies are applied in the production of fuselage components and support structures, jet engines, as well as satellites and space probes [19, 23].

In the automotive industry, weight reduction is essential for improving performance, reducing fuel consumption, and extending the range of electric vehicles [14, 26]. Traditional structural components made of solid materials are characterized by high mass, which negatively affects energy efficiency. The use of lattice and chambered structures in chassis systems, suspension systems, and load-bearing components enables weight reduction while maintaining high mechanical strength [10, 11].

Thanks to additive manufacturing techniques, manufacturers can produce components with optimized geometries that not only reduce vehicle load but also improve aerodynamics and safety. Lattice structures are also used in engine cooling systems, braking systems, and exhaust systems, where an increased heat exchange surface enhances thermal efficiency [4, 25]. Studies conducted by Aboulkhair et al. demonstrated that optimizing lattice structures in fuselage elements and support structures increases their resistance to thermal stresses [21].

The incorporation of lattice structures into automotive chassis systems, suspension systems, and load-bearing components enables weight reduction while maintaining high strength [2, 9]. Additionally, these structures are utilized in engine cooling systems and exhaust systems, where an increased heat exchange surface enhances thermal efficiency [14].

Additive manufacturing technologies have also revolutionized regenerative medicine and orthopedics by enabling the production of personalized implants and prostheses tailored to individual patient needs [18, 26]. Lattice and chambered structures are employed in bone implants because they facilitate tissue ingrowth and accelerate integration with the body. As reported by Tan et al., 3D-printed lattice implants made from bioactive materials improve the process of osseointegration and reduce the risk of rejection [28].

Moreover, 3D printing enables the fabrication of implants with complex porous architectures. Lattice structures allow for precise control of implant stiffness and elasticity, which is crucial in the case of joint endoprostheses and spinal implants [6, 13].

In the energy sector, heat exchange efficiency is crucial for the performance of cooling and heating systems. Lattice structures used in heat exchangers increase the heat transfer surface area while simultaneously reducing flow resistance and the overall weight of the structure [4]. Experiments conducted by Al-Ketan et al. demonstrated that the use of optimized lattice structures in gas turbines improves their efficiency by 15% compared to conventional cooling methods [22].

3D printing enables precise design of internal channels, allowing for the optimization of fluid and gas flow in cooling systems for turbines, reactors, and industrial installations [19]. Lattice structures are also applied in high-pressure pipelines, where they enhance resistance to internal pressure and dynamic loads [5].

The quality and mechanical strength of components manufactured using additive technologies depend on a range of 3D printing process parameters that influence both the micro- and macrostructure of the component [2, 6, 25]. Proper configuration of these parameters is crucial for optimizing tensile, compressive, bending, and fatigue strength [9, 11].

A particularly important aspect is the anisotropy of mechanical properties, meaning that the strength of a component depends on the orientation of layers relative to the direction of applied forces [10, 29, 35, 36]. Infill density affects the strength-to-weight ratio as well as the stiffness of the structure [16, 18].

While full infill provides maximum strength, it also increases weight and printing time; in contrast, lattice structures enable significant weight reduction while maintaining adequate load-bearing capacity [4, 26]. Improper printing temperature settings may lead to insufficient interlayer bonding or the formation of internal thermal stresses, which weaken the structural strength of the component [12, 13].

The aim of this study is to analyze the resistance of chamber-structured pipe conduits to external loads, including bending and compression induced by external forces. These structures were compared with solid materials in terms of their strength-to-weight ratio, allowing for the identification of an optimal cross-section that minimizes mass while maintaining high load resistance.

The results of this analysis may contribute to the optimization of the design of lightweight and durable pipe conduits for applications in modern industry.

2. MATERIALS AND METHODS

Strength tests under three-point bending and compression were conducted at the Laboratory of Materials and Structural Testing at Bydgoszcz University of Science and Technology. The three-point bending test was performed using an INSTRON 5966 universal testing machine, while the compression test was carried out on an INSTRON 8501 machine. The parameters recorded during both tests were force and displacement values.The infill structures were based on fundamental geometric shapes, namely triangles, circles, and squares. These geometries were selected because they facilitate model development, computational analysis, and finite element method (FEM) simulations.

Tab. 1. Overall dimensions and mass of the bending test specimens

Specimen structure	Geometrical dimensions			
	length l [mm]	width d [mm]	height h [mm]	mass [g]
ladder	190	30	10	26.08
triangular	190	30	10	27.17
tubular	190	30	10	33.28
solid	190	30	10	60.42

Tab. 2. Geometrical parameters of the ladder and triangular infill structures

Specimen structure	Geometrical dimensions			
	outer wall thickness [mm]	inner wall thickness [mm]	spacing between elements [mm]	number of internal walls
ladder	1.6	0.8	4.00	40
triangular	1.6	0.8	3.93	40

Tab. 3. Geometrical parameters of the tubular infill structure

Specimen structure	Geometrical dimensions			
	outer wall thickness, mm	inner wall thickness, mm	inner diameter of the tubes, mm	number of tubes
tubular	1,6	0,8	5,2	28

Preliminary tests—three-point bending—were conducted on specimens manufactured using additive technology from ABS (acrylonitrile butadiene styrene). Four variants of specimens were used in the study, each characterized by a different infill structure: ladder-type (Fig.1a), triangular (Fig. 1b), tubular (Fig. 1c), and solid (Fig. 1d), which also resulted in different masses of the elements (Table 1). The geometric dimensions of the test specimens are presented in Figure 1 and Tables 1-3.

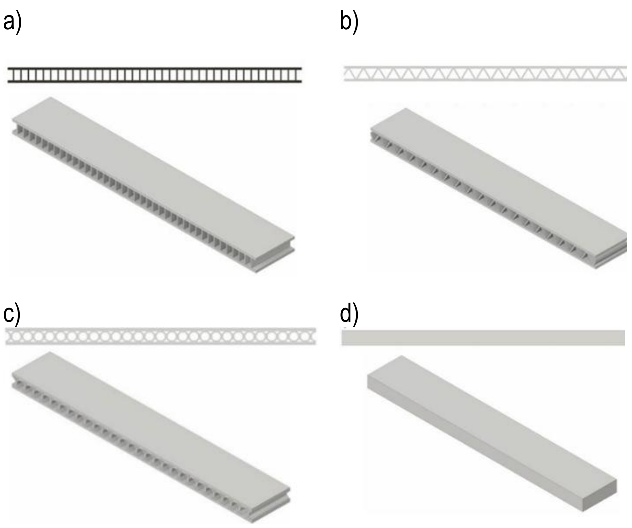

Fig. 1. Flat test specimens: a) ladder; b) triangular; c) tubular; d) solid

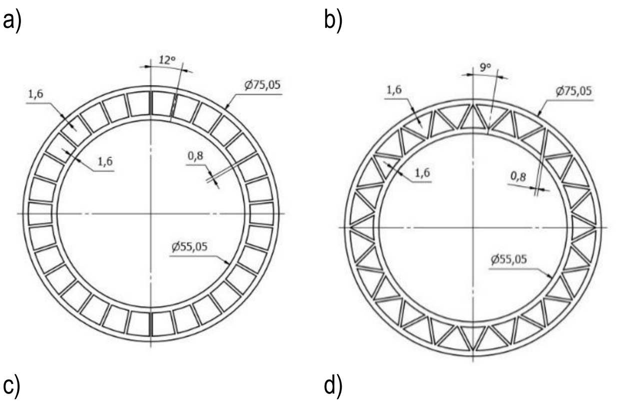

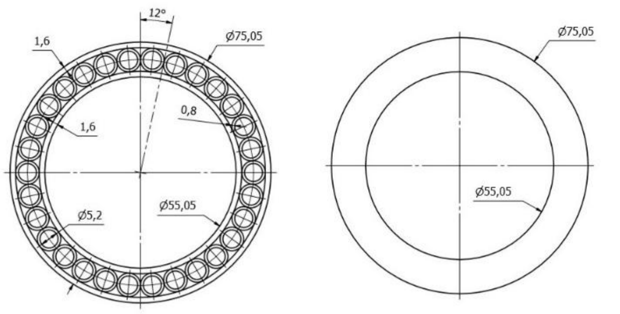

Fig. 2. Pipe specimens with: a) ladder; b) triangular; c) tubular; d) solid infill configurations

The main compression tests of tubular structural elements were also conducted on four types of ABS specimens with different infill structures: ladder-types (Fig. 2a), triangular (Fig. 2b), tubular (Fig. 2c), and solid (Fig. 2d). The length of the elements was equal to 69 mm. The compression rate was set to 0.5 mm/s for, and the tests were stopped when the specimen fractured.

3. PRELIMINARY TESTS

The static three-point bending test enabled the determination of force–displacement curves, as shown in Figure 3. Table 4 presents the maximum values of force and displacement for the four types of specimens at the initial stage, at 50% displacement, and at failure.

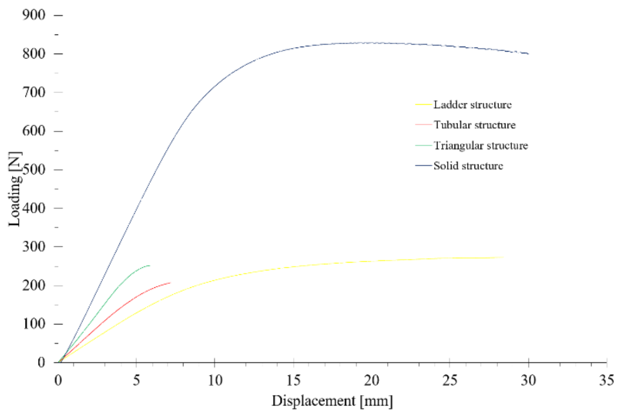

Fig. 3. Force–displacement curves for the ladder, tubular, triangle and solid structures in the three-point bending test

Tab. 4. Mean force and displacement values for four specimen types at initial, 50% deflection, and failure stages

Measurement type	Ladder structure	Tubular structure	Triangle structure	Solid structure
Initial parameters				
Loading [N]	1.07	1.09	1.28	0.05
Displacement [mm]	0.00	0.00	0.00	0.00
Measurement of 50% deflection concerning the specimen fracture				
Loading [N]	244.85	128.41	149.50	813.18
Displacement [mm]	14.21	3.54	2.91	14.85

Deflection maximum values				
Loading [N]	272.90	207.16	251.03	799.79
Displacement [mm]	28.41	7.17	5.84	30.00

The analysis of the obtained results indicates that the specimen with a solid infill structure exhibits the highest mechanical resistant, with a maximum force exceeding 800 N and a displacement of 30 mm. The solid structure provides the best mechanical properties; however, this comes at the cost of increased specimen mass.

Specimens with lattice structures are characterized by significantly lower mechanical response, but they may offer a better strength-to-weight ratio. The ladder-type structure achieves the second-highest loading capacity among the lattice variants (272.90 N) and the greatest allowable displacement among the lightweight structures (28.41 mm). The ladder geometry provides good load-bearing capacity while reducing mass by 34.34 g compared to the solid specimen.

The triangular structure exhibits a maximum load of 251.03 N, approximately 20 N lower than the ladder-type structure, with a maximum displacement of 5.84 mm. The lower displacement at failure indicates reduced deformation capacity prior to failure. The tubular structure shows the lowest loading capacity (207.16 N) and a relatively small displacement at failure (7.17 mm), indicating a limited ability to withstand bending loads compared with the other investigated structures.

In summary, the solid structure provides the highest load-bearing capacity, whereas lattice structures offer a compromise between strength and weight reduction. The selection of an appropriate infill structure should depend on specific application requirements, such as the need to minimize weight while maintaining adequate mechanical strength.

4. MECHANICAL TESTING OF PIPE CONDUITS

The presented graphs (Fig. 4) illustrate the results of compression tests of tubular elements printed from ABS using different infill structures (lattice structures). The study included specimens with ladder-type, triangular, and tubular infill, while solid specimens (full structure) were used as a reference. The aim of the analysis was to evaluate the load-bearing capacity and deformation behaviour of elements subjected to axial loading

Based on the analysis of the graphs, it was found that elements with ladder-type structures (specimens 2 and 3) exhibit very high load-bearing capacity, reaching load values close to 18–20 kN at relatively small displacements (approximately 2–3 mm). Specimen 1 failed prematurely at a significantly lower load (approximately 4 kN), which may indicate a structural defect or irregularities in the printing process.

The curves indicate a limited deformation response compared to the other structures. The ladder-type structure demonstrates nearly the same load-bearing capacity as the solid structure, suggesting that, despite its significantly lower mass, it may effectively replace solid material in applications requiring high load-bearing performance. Both the solid and ladder-type structures exhibit the smallest displacements at failure, indicating a reduced deformation capacity under bending loads.

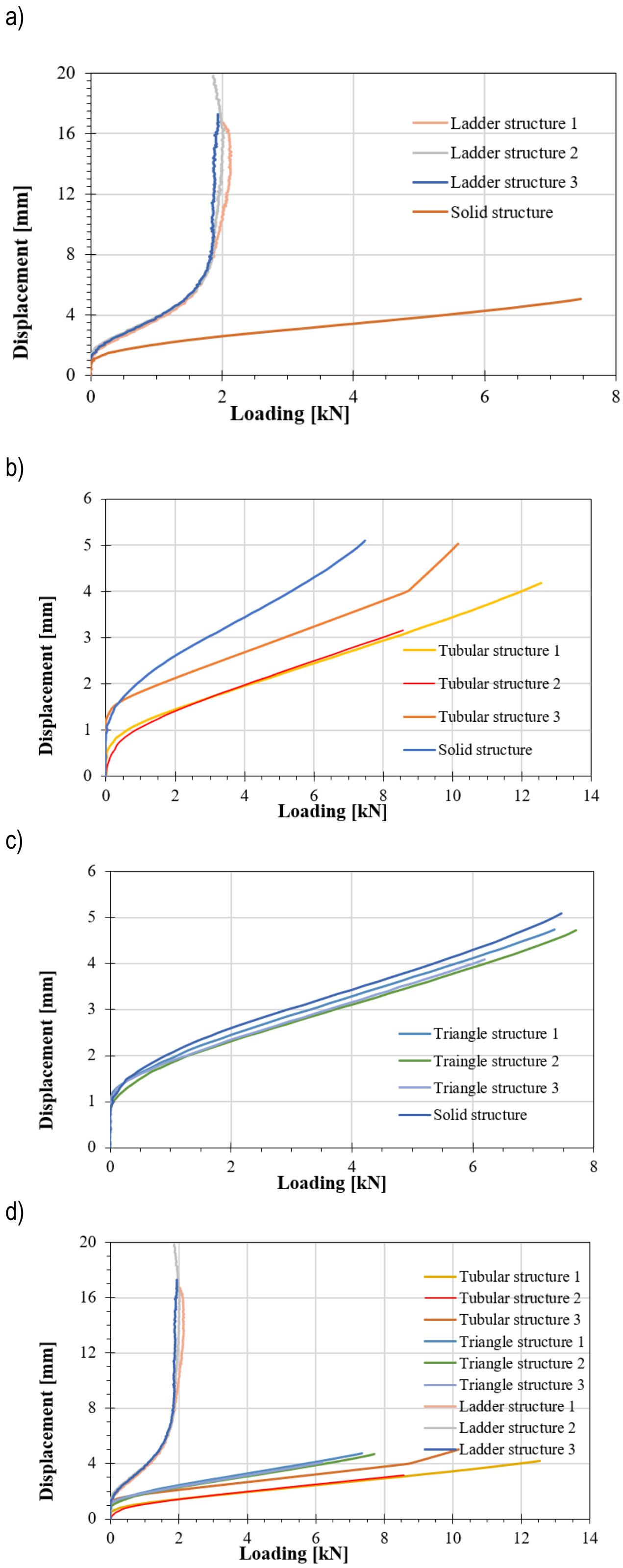

Fig. 4. Comparison of test results for: a) ladder-type, b) triangular, c) tubular, and d) all specimens

Specimens with triangular infill achieved average maximum load values of approximately 5–6 kN, indicating higher load-bearing capacity than the tubular structure. The gradual increase in force without sudden drops suggests better resistance to failure compared to the tubular configuration. These specimens exhibit relatively large displacements (5–8 mm), indicating greater flexibility compared to the ladder-type infill. The triangular structure reaches only about 25–30% of the load-bearing capacity of the solid structure, suggesting significantly lower efficiency in carrying compressive loads. It also shows greater deformation than the solid structure, reflecting higher flexibility.

All specimens with tubular infill achieved significantly lower maximum loads (3–5 kN) compared to the other structures. Specimens 1 and 2 exhibited large displacement values prior to sudden failure (over 10 mm). A rapid drop in force after reaching the peak value indicates a rapid structural failure after reaching the maximum load and high susceptibility to brittle fracture. The tubular structure demonstrates the lowest load-bearing capacity (3–5 kN), corresponding to only 15–25% of the solid structure's capacity, confirming its poor resistance to compression.

Among the investigated lattice configurations, the ladder-type structure exhibited the highest load-bearing capacity. During compression tests, specimens with this geometry reached loads of approximately 18–20 kN at displacements of about 2–3 mm, approaching the performance of the solid structure while maintaining a substantially lower mass. The ladder specimen weighed 26.08 g, compared to 60.42 g for the solid specimen, corresponding to a mass reduction of approximately 56.8%. The gradual force–displacement response observed for the ladder-type specimens indicates a progressive failure process and efficient load transfer through the structure.

The triangular structure achieved intermediate performance, reaching maximum loads of approximately 5–6 kN and displacements in the range of 5–8 mm. With a mass of 27.17 g, representing a reduction of approximately 55.0% relative to the solid specimen, this geometry achieved only about 25–30% of the load-bearing capacity of the solid structure. These results suggest that the triangular geometry may provide a compromise between weight reduction and load-bearing performance.

The tubular structure demonstrated the lowest load-bearing capacity, with maximum loads ranging from 3 to 5 kN and displacements exceeding 10 mm before failure. Although its mass was reduced to 33.28 g (approximately 44.9% lower than that of the solid specimen), the load-bearing capacity corresponded to only 15–25% of that achieved by the solid structure. Furthermore, a rapid drop in force after reaching the peak load indicates sudden structural failure and limited ability to sustain additional loading after the onset of instability. Consequently, triangular and tubular infill patterns may be less suitable for applications requiring high axial load-carrying capacity.

Considering both mass and load-bearing performance, the ladder-type structure provided the most favorable balance between structural efficiency and weight reduction. While its mass was reduced by more than half compared to the solid specimen, its maximum load remained close to that of the reference structure, indicating a significantly improved load-bearing-capacity-to-weight ratio.

The finite element method (FEM) was applied to investigate the effect of infill geometry on the displacement response of thin-walled tubular elements subjected to compressive loading. Unlike the experimental compression tests, which were evaluated based on the maximum load-bearing capacity, the FEM analysis focused on the relationship between the applied load and the resulting displacement. Therefore, the numerical assessment was based on the force-to-displacement ratio $R = P/f$, which characterizes the structural response under elastic loading conditions rather than the maximum load sustained before failure.

Simulations were carried out in the SolidWorks Simulation environment using linear static analysis (Fig. 5). Three-dimensional models of elements with identical external dimensions were developed, incorporating ladder-type, triangular, tubular, and solid infill structures. The grips of the testing machine were also modelled to reproduce the experimental boundary conditions. The influence of chamber geometry on displacement was analysed for compressive loads of 1000 N, 2000 N, and 4000 N.

The results showed a linear relationship between load and displacement for all investigated geometries, confirming elastic behaviour within the analysed loading range. The smallest displacements were observed for the solid structure. Among the lattice structures, the tubular infill exhibited the lowest displacement values, followed by the triangular and ladder-type configurations. These results indicate that chamber geometry significantly influences the displacement response of the structure under compressive loading.

To compare the numerical and experimental results, the force-to-displacement ratio $R = P/f$ was introduced, where P is the applied force and f is the measured displacement. A higher value of R indicates a smaller displacement under a given load. It should be emphasized that parameter R does not represent the maximum load-bearing capacity of the structure and therefore should not be directly compared with the maximum loads obtained in the compression experiments. Instead, it was used as a qualitative indicator of the structural response under loading and as a basis for comparing FEM predictions with experimental observations.

Both the experimental and numerical analyses produced the same ranking with respect to parameter R, with the tubular structure exhibiting the highest force-to-displacement ratio, followed by the triangular and ladder-type configurations. However, the ranking based on maximum load-bearing capacity obtained from compression tests was different, with the ladder-type structure achieving the highest loads. This discrepancy arises because the two approaches evaluate different performance criteria: the experimental results are based on maximum load before failure, whereas parameter R characterizes the displacement response under load. Consequently, the FEM results should be interpreted as a qualitative assessment of structural behaviour rather than a direct prediction of failure load.

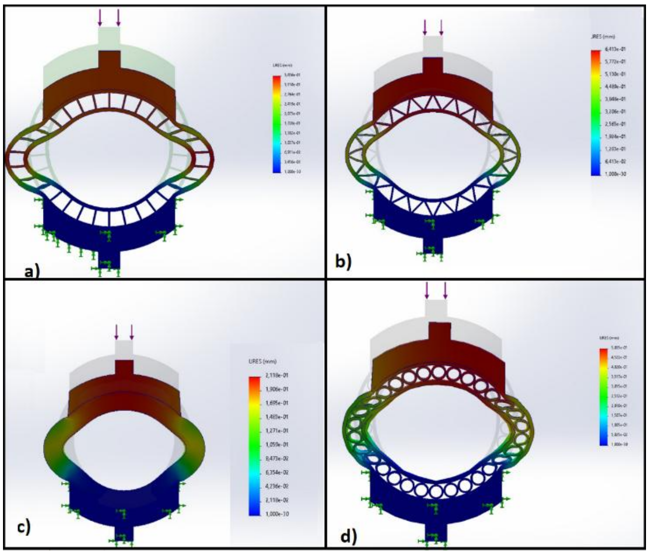

Fig. 5. Representative FEM simulations: a) ladder-type infill, F = 1900 N; b) triangular infill, F = 7700 N; c) solid infill, F = 7500 N; d) tubular infill, F = 8600 N

The results of the first analysis are presented in Table 6. A total of 12 simulations were performed. Simulations were conducted for each chamber geometry, with compressive loads of 1000 N, 2000 N, and 4000 N applied.

Tab. 5. Simulation parameters

Simulation parameters	
Analysis type	Static analysis
Mesh type	Solid mesh
System of units	SI (MKS)
Length/Displacement	mm
Pressure/Stress	N/m²
Material of the grips	Carbon steel (St3S)
Material of thin-walled tubes	ABS

Tab. 6. FEM results for thin-walled tubes

Measurement type	Ladder structure	Tubular structure	Triangle structure	Full structure
Loading [N]	1000			
Displacement [mm]	0.18	0.05	0.08	0.02
Loading [N]	2000			
Displacement [mm]	0.36	0.11	0.16	0.05
Loading [N]	4000			
Displacement [mm]	0.72	0.23	0.33	0.11

Based on the results presented in Table 6, the characteristic relationship $f(F) = \delta$ (Fig. 6) was developed for thin-walled tubes with triangular, tubular, ladder-type, and solid chamber infill. The obtained curves are linear functions, each with a different slope.

The plot indicates that the type of chamber infill significantly affects the displacement response under compressive loading. The solid structure exhibited the smallest displacements under the applied loads. Among the lattice structures, the tubular configuration showed the lowest displacement values, followed by the triangular and ladder-type structures. These results reflect differences in deformation response and should not be interpreted as a ranking of load-bearing capacity.

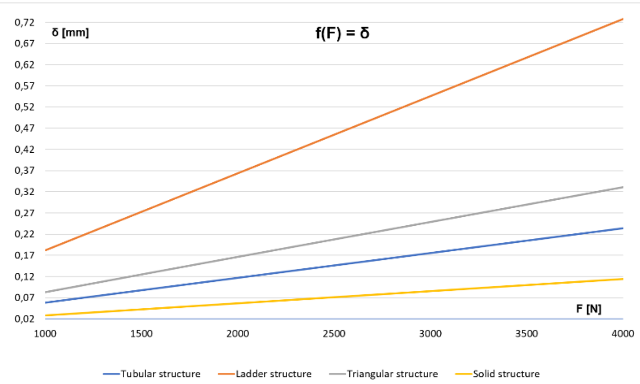

Fig. 6. Characteristic $f(F)=\delta$ for specimens with tubular, ladder-type, triangular, and solid infill

To compare the experimental results with the FEM results, a parameter describing the force-to-deflection ratio of the model was determined. The parameter was calculated according to the following equation:

$$R = \frac{P}{f} \tag{1}$$

where:
R – force-to-displacement ratio,
P – force,
f – displacement.

The parameter represents a coefficient describing the relationship between the applied force and the measured deflection. The results of the comparative analysis are qualitative in nature. The parameter was defined to enable a qualitative comparison between experimental results and FEM simulations.

In the static FEM approach, the phenomenon of specimen fracture cannot be observed. Therefore, a reliable basis for comparison is the determination of the force-to-deflection ratio of the model. In the subsequent part of the analysis, parameters obtained from experimental tests and FEM simulations will be compared.

Table 7 presents the strength results of selected geometric structures of thin-walled tubes obtained from experimental tests and FEM simulations. The table includes the parameter R, which describes the force-to-displacement ratio of the specimen subjected to compression under external loading.

Tab. 7. Experimental and FEM results of the force-to-displacement ratio (R) for the investigated infill geometries

Specimens	R	F experimental	P experimental	F FEM	P FEM
	kN/mm	mm	kN	mm	kN
tubular K6	10.2	5.024	2.03	0.60	17.11
tubular K5	8.6	3.154	2.73	0.50	17.20
tubular K4	12.6	4.117	3.06	0.74	17.03
triangular T3	6.2	4.090	1.52	0.50	12.40
triangular T2	7.7	4.716	1.63	0.64	12.03
triangular T1	7.4	4.733	1.56	0.61	12.13
ladder P3	1.9	19.267	0.10	0.34	5.59
ladder P2	2.0	16.625	0.12	0.36	5.56
ladder P1	1.9	17.115	0.11	0.34	5.59

Both the experimental tests and FEM simulations produced the same ranking of the investigated chamber geometries. In both approaches, the tubular structure exhibited the highest force-to-displacement ratio (R), followed by the triangular and ladder-type structures. The average experimental values of R were 10.47, 7.10, and 1.93 kN/mm for the tubular, triangular, and ladder-type structures, respectively, while the corresponding FEM values were 17.11, 12.19, and 5.58 kN/mm. Although the FEM model overestimated the absolute values of the parameter R, it correctly reproduced the relative performance of the investigated geometries. These results indicate qualitative agreement between the experimental and numerical approaches and confirm that FEM can be used as a useful tool for preliminary assessment and comparison of alternative chamber geometries.

5. RESULTS DISCUSSION

The conducted experimental studies and numerical analyses enabled the assessment of the influence of chambered infill geometry on the mechanical properties of thin-walled tubular elements manufactured using additive technology from ABS material. The results clearly indicate that the internal structure plays a key role in determining the load-bearing capacity and deformation response of the structure, as well as its failure behavior.

Figure 7 presents the $f(F) = \delta$ characteristic for specimens with tubular, ladder-type, triangular, and solid infill. In the three-point bending tests, specimens with a solid structure exhibited the highest load-bearing capacity, which is consistent with classical strength of materials theory—a homogeneous cross-section provides the greatest moment of inertia and a uniform stress distribution. However, achieving maximum load-bearing capacity is associated with a significant increase in component mass, which in many engineering applications constitutes a limiting factor.

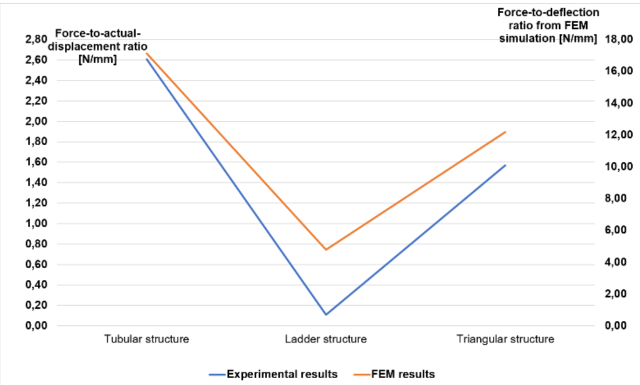

Fig. 7. Characteristic $f(F) = \delta$for specimens with tubular, ladder-type, triangular, and solid infill

Among the lattice structures, the ladder-type configuration exhibited the best bending performance, reaching a maximum load of 272.90 N at a displacement of 28.41 mm. Compared with the other lattice configurations, this structure maintained a relatively high load-bearing capacity while undergoing the largest displacement before failure. The triangular structure reached a maximum load of 251.03 N at a displacement of 5.84 mm, indicating a lower deformation capacity prior to failure. The tubular structure exhibited the lowest load-bearing capacity, reaching a maximum load of 207.16 N and a displacement of 7.17 mm at failure. The reduced performance of the tubular configuration may be associated with local instability of thin-walled elements and stress concentrations at the interfaces between adjacent chambers.

Different trends were observed in the axial compression tests. The ladder-type structure achieved maximum loads of approximately 18–20 kN while maintaining a substantially lower mass than the solid specimen (26.08 g and 60.42 g, respectively). This result suggests efficient transfer of compressive loads through the vertically oriented structural members. The triangular structure exhibited intermediate performance, reaching maximum loads of approximately 5–6 kN and displacements in the range of 5–8 mm before failure. In contrast, the tubular structure demonstrated the lowest load-bearing capacity, with maximum loads ranging from 3 to 5 kN. In addition, the force–displacement curves showed a rapid decrease in load after reaching the peak value, indicating sudden failure of the structure. The reduced load-bearing performance of the tubular configuration may be associated with local instability of the chamber walls and stress concentrations within the lattice geometry.

The FEM simulations reproduced the displacement-response trends of the investigated geometries. However, the ranking based on the force-to-displacement ratio (R) differed from the ranking based on the maximum load-bearing capacity obtained experimentally, since these criteria describe different aspects of structural performance. At the same time, quantitative discrepancies between simulation and experimental results were observed, resulting from the limitations of the applied linear model. The simulations did not account for nonlinear phenomena such as local buckling, material degradation, contact friction, or anisotropy arising from the 3D printing process.

An important factor contributing to these discrepancies may also be the layered structure of ABS material produced using FDM technology, which introduces directional variability in mechanical properties. Real specimens also exhibit structural inhomogeneities, pores, and imperfections resulting from the printing process, which may initiate failure at lower loads than those predicted numerically.

The obtained results confirm that appropriate selection of infill geometry significantly improves the strength-to-weight ratio. Lattice structures, particularly those with a ladder-type configuration, can serve as an attractive alternative to solid components in applications requiring high load-bearing capacity combined with reduced weight, such as in transportation, aerospace, or energy sectors. In motorsports, such components are especially desirable due to the strong influence of the strength-to-weight ratio on performance outcomes.

6. CONCLUSIONS

Based on the conducted experimental investigations and FEM simulations, the following conclusions can be drawn:

– The geometry of the chambered infill significantly influences the load-bearing capacity and deformation response of thin-walled tubular elements manufactured from ABS using FDM technology. Different infill configurations resulted in substantial differences in mechanical performance under both bending and compressive loading conditions.
– The solid structure exhibited the highest load-bearing capacity in bending tests, reaching a maximum load of 799.79 N. However, this configuration was also characterized by the highest mass (60.42 g), which may limit its application in lightweight structural systems.
– Among the investigated lattice configurations, the ladder-type structure demonstrated the most favorable overall performance. In bending tests it reached a maximum load of 272.90 N, while in compression tests it achieved loads of approximately 18–20 kN, approaching the performance of the solid structure despite a mass reduction of approximately 56.8%.
– The triangular structure provided intermediate performance, combining moderate load-bearing capacity with significant weight reduction. This geometry may therefore represent a practical compromise between structural efficiency and mass reduction in applications where maximum load capacity is not the primary design requirement.

- The tubular structure exhibited the lowest load-bearing capacity in both bending and compression tests. Maximum compressive loads ranged from approximately 3 to 5 kN, and the force–displacement curves indicated sudden failure after reaching peak load, suggesting limited suitability for applications requiring high axial load-carrying capacity.
- The FEM simulations successfully reproduced the displacement response of the investigated geometries under compressive loading. However, the ranking obtained from the force-to-displacement ratio $R = P/f$ differed from the ranking based on experimentally determined maximum loads because these criteria describe different aspects of structural performance.
- The numerical model should be considered a qualitative tool for assessing structural response rather than a direct predictor of failure loads. Quantitative discrepancies between simulations and experiments are attributed to the use of linear static analysis and the omission of nonlinear phenomena such as local buckling, material failure, contact effects, and manufacturing-induced anisotropy.
- The obtained results confirm that appropriately designed lattice structures can provide a favorable load-bearing-capacity-to-weight ratio. In particular, the ladder-type configuration appears to be a promising solution for lightweight engineering applications requiring high mechanical efficiency combined with substantial weight reduction.

REFERENCES

1. Alafaghani A et al. Experimental optimization of fused deposition modelling processing parameters: A design-for-manufacturing approach. Mater Des. 2017;151:216-225.
2. Domingo-Espin M, et al. Mechanical property characterization and simulation of fused deposition modeling polycarbonate parts. Mater Des. 2015;83:670-682.
3. Gibson LJ, Ashby MF. Cellular solids: structure and properties. 2nd ed. Cambridge: Cambridge University Press; 1997.
4. Hossain MS, et al. Structure, electronic structure, optical and magnetic studies of double perovskite Gd_2MnFeO_6 nanoparticles: First principle and experimental studies. Mater Today Commun. 2020;25:101603.
5. Huang J, et al. Thermally assisted 3D printing of biopolymer with high solute loading and improved mechanical properties. Addit Manuf. 2022;59:103088.
6. Letcher T, Waytashek M. Material property testing of 3D-printed specimens in PLA on an entry-level 3D printer. Addit Manuf. 2014;2:64-72.
7. Kumar E, Liang J, Xiao F. A machine learning framework for rapid design of polymer nanocomposites with specific mechanical properties. Mater Des. 2020;195:109026.
8. Maskery I et al. Compressive failure modes and energy absorption in additively manufactured double gyroid lattices. Addit Manuf. 2017;16:1-10.
9. Rane K, Strano G. A comprehensive review of extrusion-based additive manufacturing processes for rapid production of metallic and ceramic parts. Prog Addit Manuf. 2019;4(2):123-142.
10. Rankouhi B et al. Failure analysis and mechanical characterization of 3D printed ABS with respect to layer thickness and orientation. J Fail Anal Prev. 2016;16:467-481.
11. Spoerk M, et al. Optimisation of the adhesion of polypropylene-based materials during extrusion-based additive manufacturing. Polymers. 2018;10(5):490.
12. Turner BN, Strong R, Gold SA. A review of melt extrusion additive manufacturing processes: I. Process design and modeling. Rapid Prototyp J. 2014;20(3):192-204. https://doi.org/10.1108/RPJ-01-2013-0012
13. Vaezi M, Yang S. Extrusion-based additive manufacturing of PEEK for biomedical applications. Mater Sci Eng C. 2015;57:451-463.
14. Wang X et al. A material removal model for nonconstant-contact flexible grinding process. Int J Adv Manuf Technol. 2021;114:1953-1966.
15. Yang L et al. FullControl GCode Designer: Open-source software for unconstrained design in additive manufacturing. Addit Manuf. 2021;46:102109.
16. Yao T et al. In situ investigation into temperature evolution and heat generation during additive friction stir deposition: A comparative study of Cu and Al-Mg-Si. Addit Manuf. 2020;34:101386.
17. Zhang X, et al. Multiscale bioprinting of vascularized models. J Mech Behav Biomed Mater. 2019;96:204-216.
18. Zanjanijam AR, et al. Progress in manufacturing and properties of additive manufacturing of PEEK: A review. Prog Mater Sci. 2020;116:100636.
19. Zhu Y, et al. Site occupancy of alloying elements in the L12 structure determined by channeling enhanced microanalysis in γ/γ' Co-9Al-9W-2X alloys. Acta Mater. 2019;177:176-188.
20. Zohdi TI. A hierarchical framework for modeling particulate agglomeration and deposition. Comput Mech. 2017;59:277-295.
21. Aboulkhair NT, Simonelli M, Parry L, Ashcroft I, Tuck C, Hague R. 3D printing of aluminium alloys: Additive manufacturing of aluminium alloys using selective laser melting. Prog Mater Sci. 2019;106:100578. https://doi.org/10.1016/j.pmatsci.2019.100578
22. Al-Ketan O, et al. Forced convection computational fluid dynamics analysis of architected and three-dimensional printable heat sinks based on triply periodic minimal surfaces. Energy Convers Manag. 2018;174:461-478.
23. Gardan J. Smart materials in additive manufacturing: State of the art and trends. Virtual Phys Prototyp. 2019;14(1):1-18. https://doi.org/10.1080/17452759.2018.1518016
24. Ghouse S, Babu S, Nai K, Hooper PA, Jeffers JRT. The influence of laser parameters, scanning strategies and material on the fatigue strength of a stochastic porous structure. Addit Manuf. 2018;22:290-301. https://doi.org/10.1016/j.addma.2018.05.024
25. Goh GD, Yap YL, Tan HK, Yeong WY. Process-property relationships in digital light processing of functional materials. Addit Manuf. 2020;30:100846.
26. Ligon SC, Liska R, Stampfl J, Gurr M, Mülhaupt R. Polymers for 3D printing and customized additive manufacturing. Chem Rev. 2017;117(15):10212-10290.
27. Ngo TD, Kashani A, Imbalzano G, Nguyen KT, Hui D. Additive manufacturing (3D printing): A review of materials, methods, applications, and challenges. Compos Part B Eng. 2018;143:172-196.
28. Tan X, Moetazedian A, Gleadall A, Silberschmidt VV. Effect of environment on mechanical properties of 3D printed polylactide for biomedical applications. J Mech Behav Biomed Mater. 2020;102:103510.
29. Kumar S, Kruth JP. Composites by rapid prototyping technology. Mater Des. 2010;31(2):850-856.
30. DebRoy T, Wei HL, Zuback JS, Mukherjee T, Elmer JW, Milewski JO, et al. Additive manufacturing of metallic components – Process, structure and properties. Progress in Materials Science. 2018;92:112–224. https://doi.org/10.1016/j.pmatsci.2017.10.001
31. Zheng X, Lee H, Weisgraber TH, Shusteff M, DeOtte J, Duoss EB et al. Ultralight, ultrastiff mechanical metamaterials. Science. 2014;344(6190):1373–1377. https://doi.org/10.1126/science.1252291
32. Berger JB, Wadley HNG, McMeeking RM. Mechanical metamaterials at the theoretical limit of isotropic elastic stiffness. Nature. 2017;543:533–537.https://doi.org/10.1038/nature21075
33. Liu J, Gaynor AT, Chen S, Kang Z, Suresh K, Takezawa A, et al. Current and future trends in topology optimization for additive manufacturing. Structural and Multidisciplinary Optimization. 2018;57:2457–2483. https://doi.org/10.1007/s00158-018-1994-3
34. Bendsøe MP, Sigmund O. Topology Optimization: Theory, Methods, and Applications. Springer; 2003. https://doi.org/10.1007/978-3-662-05086-6
35. Torrado Perez AR, Roberson DA, Wicker RB. Fracture surface analysis of 3D-printed tensile specimens of novel ABS-based materials. Journal of Failure Analysis and Prevention. 2014;14:343–353.

https://doi.org/10.1007/s11668-014-9803-9
36. Chacón JM, Caminero MA, García-Plaza E, Núñez PJ. Additive manufacturing of PLA structures using fused deposition modelling: Effect of process parameters. Materials & Design. 2017;124:143–157.https://doi.org/10.1016/j.matdes.2017.03.065
37. Gibson LJ. Biomechanics of cellular solids. Journal of Biomechanics. 2005;38(3):377–399. https://doi.org/10.1016/j.jbiomech.2004.09.027
38. Yan C, Hao L, Hussein A, Raymont D. Evaluations of cellular lattice structures manufactured using selective laser melting. International Journal of Machine Tools and Manufacture. 2012;62:32–38. https://doi.org/10.1016/j.ijmachtools.2012.06.002

Grzegorz Szala: https://orcid.org/0000-0001-5398-2405

Karolina Karolewska: https://orcid.org/0000-0001-9885-2022

Maciej Janiec: https://orcid.org/0000-0001-6772-5450